Int J Adv Manuf Technol (2014) 73:1073–1079
DOI 10.1007/s00170-014-5857-9

ORIGINAL ARTICLE

Influences of rotation speed on microstructures and mechanical properties of 6061-T6 aluminum alloy joints fabricated by self-reacting friction stir welding tool

J. C. Hou · H. J. Liu · Y. Q. Zhao

Received: 26 September 2013 / Accepted: 11 April 2014 / Published online: 11 May 2014

Abstract A 6061-T6 aluminum alloy was self-reacting friction stir welded by using the specially designed tool with unequal shoulder diameters at a constant welding speed of 150 mm/min to investigate the effect of rotation speed on microstructure and mechanical properties of the joints. Excessive flash on the bottom surface of the joint and groove defects on both surfaces of the joint were formed when the lower shoulder diameter was much smaller. The suitable shoulder sizes were determined as 16 and 18 mm in lower shoulder diameter and upper shoulder diameter, respectively. The grain size and the dislocation density in the weld nugget zone (WNZ) increased with increasing rotation speed. The tensile strength of joints first increased with increasing rotating speed and then decreased remarkably as a result of the formation of void defect. The joints welded at lower rotation speeds were fractured in the thermal mechanically affected zone (TMAZ). However, the fracture locations of the defect-free joints were changed to the heat affected zone (HAZ) at higher rotation speeds.

Keywords Self-reacting friction stir welding · Shoulder diameter · Rotation speed · Mechanical properties

1 Introduction

It is difficult to join heat-treatable aluminum alloys by using fusion welding, i.e., arc welding and laser beam welding (LBW), owing to the occurrence of hot cracking and porosity [1–3]. Additionally, for the electron beam welding (EBW) process, the strengthening phases can be lost resulting from the high temperature experienced in the fusion zone, and thus the weld strength is dramatically decreased [4–6]. Friction stir welding (FSW), as a solid state joining process, can be used to produce sound joints in heat-treatable aluminum alloys [7–9]. However, conventional FSW technique is involved in the restrictions such as the requirement for significant plunge forces, the requirement for rigid clamping to prevent part movement owing to huge traversing forces, the requirement for a strong backing plate or anvil to react process loads into the fixture, and the risk of producing root defect, and thus its wide application in complex shaped large structures is limited. One of the promising ways to avoid these disadvantages is to use the self-reacting friction stir welding (SRFSW) tool which provides a bottom shoulder to take the place of the backing plate used in the conventional FSW [10–12].

Both shoulders rotate and produce frictional heat during the SRFSW process. Accordingly, the additional torque and the tension stress engaged on the pin by the lower shoulder may cause the risk of breaking the pin. Published investigations confirm that SRFSW developments are more difficult than that of conventional FSW, and SRFSW technique is difficult to increase welding speed owing to that the huge mechanical loading is engaged on the pin [13–15]. To our knowledge, little literature dealing with reducing the load on the tool to avoid the tool fracturing has been reported. Generally, the diameter of the upper shoulder is equal to that of the lower shoulder. To reduce the load on the pin, the tool with the diameter of the lower shoulder smaller than that of the upper shoulder has been invented [16]. Regarding to the heat-treatable alloys, the welding heat input can lead to the formation of soften (strength loss) zone in the FSW joints as a result of the dissolution or coarsening of the strengthening phases. In order to reduce the deterioration level of the strengthening

J. C. Hou · H. J. Liu (✉) · Y. Q. Zhao
State Key Laboratory of Advanced Welding and Joining, Harbin Institute of Technology, Harbin 150001, China
e-mail: liuhj@hit.edu.cn

J. C. Hou
School of Material Science and Technology, Shaanxi University of Technology, Hanzhong 723003, China

Table 1 Chemical composition and mechanical properties of 6061-T6 aluminum alloy

Chemical compositions (wt.%)									Mechanical properties	
Al	Si	Fe	Cu	Mn	Mg	Cr	Zn	Ti	Tensile strength (MPa)	Elongation (%)
Balance	0.4–0.8	<0.7	0.15–0.4	<0.15	0.8–1.2	0.04–0.35	<0.25	<0.15	284	14

phase, different methods have been developed, including the parameters optimization, post-heat treatment, in-process cooling using external refrigerants, submerged FSW. For instance, İpekoğlu et al. [17, 18] concluded that the post weld heat treatment could both restore the strength of the joint welded in T6 and O conditions and the abnormal grain growth occurred which were dependent on the welding parameters and the prior temper condition. To our knowledge, only limited literatures are regarding to the microstructure and the mechanical properties of the self-reacting friction stir welded joints [19–21].

For the FSW process, the parameters including rotation speed, welding speed, and plunging force have a significant effect on the material flow behavior and the temperature distribution which can determine the microstructure evolution and the resulting mechanical properties [22–24]. İpekoğlu et al. [17] reported that the hardness loss of the AA 7075-T6 FSW joints obtained at the rotation speed of 1,000 rpm and the welding speed of 150 mm/min was higher than that obtained at the rotation speed of 1,500 rpm and the welding speed of 400 mm/min. Arora et al. [25] also concluded that the strength of 2219-T87 FSW joints increased with increasing welding speed and decreased with increasing rotation speed. The reason for their results is that the increase of welding speed or the decrease of rotation speed leads to the decrease of welding heat input, and thus the deterioration level of the strengthening phases is reduced in the heat affected zone (HAZ) and thermal mechanically affected zone (TMAZ) of heat-treatable aluminum alloy joints. In this situation, the tensile strength and the minimum hardness of the FSW joints should be enhanced.

In this study, the tools with different diameters of the lower shoulders are employed in the SRFSW experiments to determine the suitable dimension of the lower shoulder, and the focus is placed on the effect of rotation speed on the microstructure and mechanical properties of the joints welded at a fixed welding speed.

2 Experimental details

Commercial 6061-T6 aluminum alloy rolled plates are adopted in the experiment with the thickness of 4 mm. The nominal chemical composition and mechanical properties are listed in Table 1. The SRFSW tool consists of two shoulders and one pin. The shoulders are characterized by a combination of cavity and fillet. The diameter of the upper shoulder is 18 mm, and the lower shoulders have three dimensions: 12, 14 and 16 mm in diameter. The pin design possesses a simple cylindrical profile with the diameter of 8 mm. During the welding, the whole plunge depth is 0.06 which is implemented on the upper shoulder and the lower shoulder equally. An indigenously designed and computer controlled FSW (FSW-3LM-003) machine is applied to fabricate the joints. According to the experience for welding the 4-mm-thick 6061-T6 aluminum alloy, process parameters with a rotation

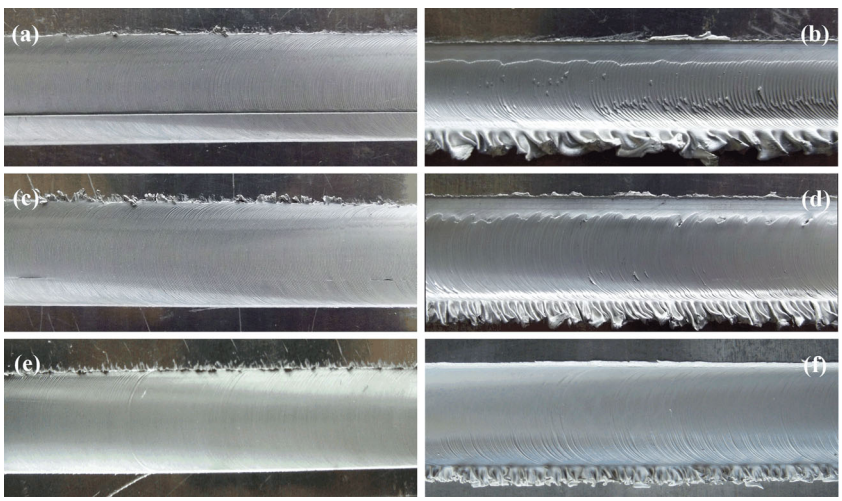

Fig. 1 Visual appearance of the joints welded by the lower shoulders with different diameters of: **a** top view, the diameter of 12 mm, **b** bottom view, the diameter of 12 mm, **c** top view, the diameter of 14 mm, **d** bottom view, the diameter of 14 mm, **e** top view, the diameter of 16 mm, and **f** bottom view, the diameter of 16 mm

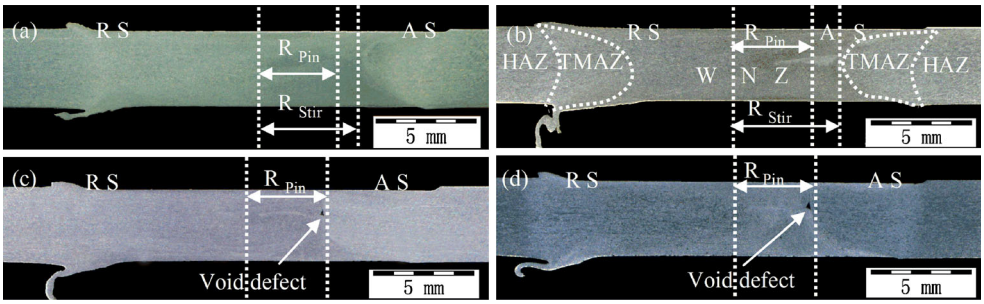

Fig. 2 Cross-sections of joints welded at different rotation speeds of **a** 400 rpm, **b** 600 rpm, **c** 700 rpm, and **d** 800 rpm

speed and welding speed of 600 rpm and 200 mm/min, respectively, are chosen to evaluate the suitability of the diameter of the lower shoulder in the welding. Then, the SRFSW is performed at a constant welding speed of 150 mm/min together with different rotation speeds of 400, 500, 600, 700, 800 rpm.

All the joints are cross-sectioned perpendicularly to the welding direction for microstructure and macrostructure analysis by using the electrical-discharge cutting machine. Metallographic samples are polished by electrolytic polishing with $HClO_4$ solution (5 % $HClO_4$ in ethanol at room temperature, under 28 V) for 15 s and are etched by the Keller's reagent. Subsequently, the specimens are observed by an optical microscope (OM; Olympus-MPG3). The average grain size is determined by the mean liner intercept technique. The Vickers hardness on the cross-section is measured at mid thickness of the joints at a spacing of 1 mm using a load of 0.98 N for 10 s.

The dislocations and precipitates are examined on sections parallel to the welding direction by using transmission electron microscopy (TEM). The TEM samples are polished on the different grades of emery paper, and then are prepared by twin-jet electropolishing using a solution of 70 % methanol and 30 % nitric at −35 °C under 18 V.

The tensile test is conducted on universal testing machine (Instron-1186) at room temperature by using a crosshead speed of 1 mm/min. The fracture features are analyzed by using the OM.

3 Results and discussion

3.1 Microstructural characteristics

Figure 1 shows the top and bottom views of the joints welded by the tools with lower shoulders of 12, 14 and 16 mm in diameter. The visible groove defect on both surfaces of the joints and excessive flash on the bottom surface of the joint are formed by using the lower shoulder of 12 mm in diameter. The weld visual quality of both surfaces is improved as the diameter of the lower shoulder is increased to 14 mm. Finally, the joint with high quality surface appearance, exhibiting smooth and defect free surfaces, is obtained as the lower shoulder is increased to 16 mm in diameter. Thus, the appropriate diameter of the lower shoulder is determined as 16 mm. If the diameter of the lower shoulder is excessively smaller than that of the upper shoulder, the plunge force introduced on the lower shoulder will be significantly smaller than that of the upper shoulder resulting in that the lower shoulder cannot produce sufficient reacting force. Therefore, a large amount of plasticized materials are extruded out, resulting in the formation of the groove defect on the upper surface of the joint, excessive flash and a groove defect on the bottom surface of the joint.

Figure 2 shows cross-sections of the joints produced at different rotation speeds. It can be seen that sound joints are produced at lower rotation speed. On the contrary, much higher rotation speed leads to the formation of the void defect. All the joints are mainly comprised of four distinct zones, i.e., WNZ (weld nugget zone), TMAZ, HAZ and BM (base material), as illustrated by the dot lines (see Fig. 2b). The geometry of the weld nugget displays a saddle shape with a width that extends from the stir zone diameter at the mid-thickness to almost the shoulder width (the actual width of plastic metal contacted with the shoulder) at the bottom and upper surfaces. In case of SRFSW, the material flow in the root region and crown region of the WNZ is mainly caused by the shoulders, while the material flow in the region of the mid thickness of the WNZ is governed by the tool pin. Consequently, the flow patter of the material near the top and bottom surface of the SRFSW joints must be different from that gained in the lower part of the WNZ resulting in the symmetric saddle shaped WNZ. As the frontier between WNZ and the TMAZ on the advance side (AS) is clear enough, it is possible to measure a

Table 2 Width of WNZ at the mid thickness of the joints formed at different rotation speeds

Rotation speed (rpm)	Width of WNZ (mm)
400	10.10
600	10.63
700	8
800	8

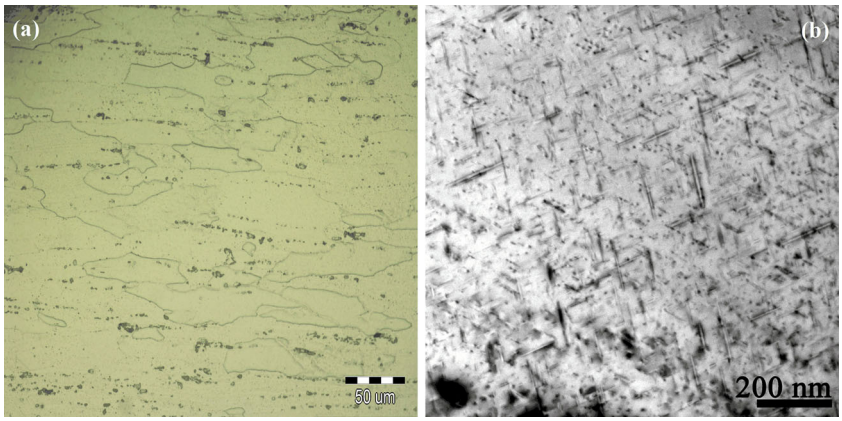

Fig. 3 Microstructrure of BM of **a** optical macrograph and **b** bright-field TEM

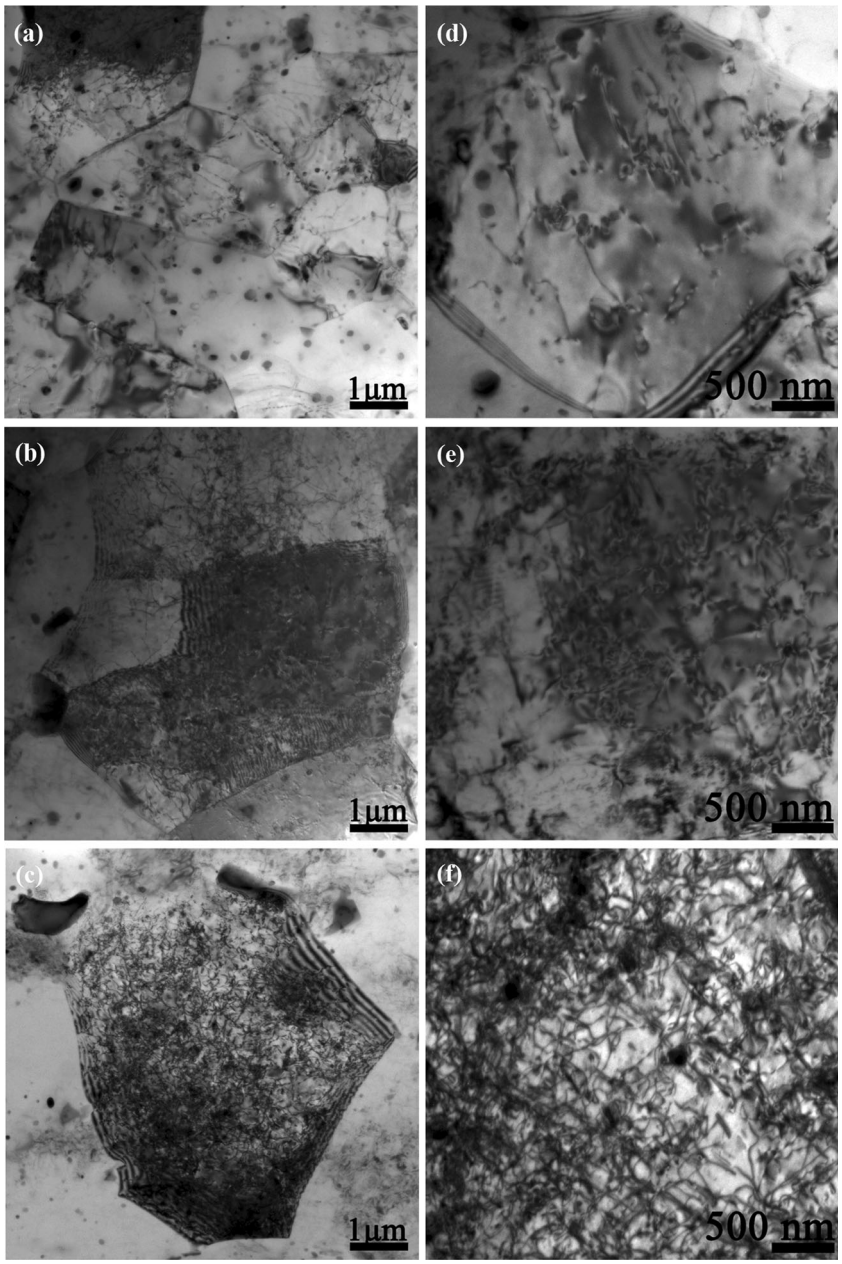

Fig. 4 Bright-field TEM of the WNZ obtained at different rotation speeds of **a** 400 rpm, **b** 500 rpm, **c** 600 rpm; **d**, **e**, **f** magnified view of **a**, **b**, **c**, respectively

half of the width at mid thickness of the WNZ. Meanwhile, the frontier between WNZ and TMAZ on the retreating side (RS) is not clear. To better understand the effect of rotation speed on the width of the WNZ, the weld center and the radius of the tool pin are given (see Fig. 2). The width at mid thickness of the WNZ is listed in Table 2, which indicates that the width is first increased with the rotation speed, and then is decreased with the increasing rotation speed. Moreover, the void defects are formed as the width of the WNZ is no bigger than the diameter of the tool pin. The demarcation between the TMAZ and WNZ obtained at lower rotation speed is sharper than that obtained at higher rotation speed. A similar profile development trend is gained with the increasing rotation speed at constant welding speed [26].

The microstructure of BM is shown in Fig. 3. The BM is characterized by coarse and elongated grains typical of hot-rolled structure. In Fig. 3b, high density fine needle-shaped precipitates and low density coarse block-shaped precipitates distributed in the BM are considered to be β'' and β' according to previous investigations [27, 28]. In addition, higher density of β'' phase showing peek aging strengthening condition results in good mechanical properties for this alloy.

In contrast to BM, the WNZ exhibits fine equiaxed grains as a result of re-crystallization (see Fig. 4a–c). Much finer grains (approximately 1 μm) are seen in the specimens obtained at the lower rotation speed of 400 rpm. As the rotation speed increases, the grains in the WNZ tend to grow dramatically, which is attributed to higher heat exposure. Moreover, it is more difficult to dissipate heat from the welding tool owing to that the lower shoulder also produce much frictional heat and no heat sink is available just like the backing plate for the conventional FSW during SRFSW.

Meanwhile, a deep observation can be made (see Fig. 4d–f) under a higher magnification. First, all metastable phases β'' and β' are diminished in the WNZ, but some block-shaped equilibrium phases are randomly distributed in WNZ irrespective of the rotation speed. This implies that the peak temperature incurred in the WNZ has surpassed the solves of β' (the solves of β' is higher than that of β''). It is well known that the mechanical properties of the heat-treated aluminium alloy depend slightly on equilibrium phase as a result of lack of coherency with the matrix. Thus, the softened region is formed in WNZ of the weld. Second, the dislocation densities increase with increasing rotation speed.

3.2 Hardness profile across the joints

The Vickers hardness distribution profiles on the transverse section of the joint are exhibited in Fig. 5. It can be inferred that all the joints have a softened region consisting of WNZ, TMAZ and HAZ irrespective of rotation speed which is attributed to precipitation evolution caused by the thermal cycle during the SRFSW. Compared to the other hardness

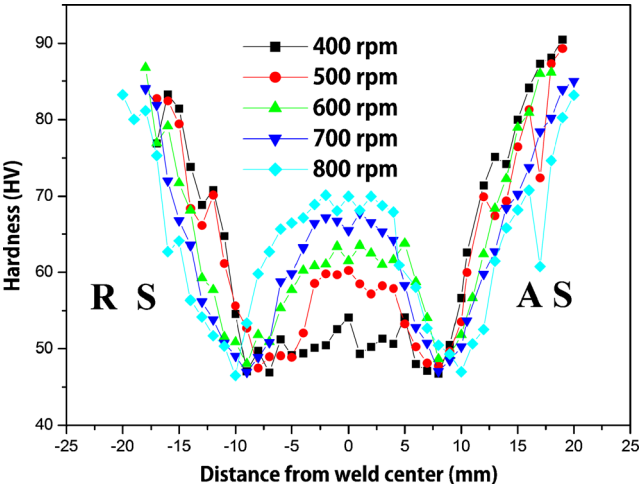

Fig. 5 Hardness distribution of the joints welded at different rotation speeds

profile in the WNZ of the joint produced at higher rotation speed, the profile in the WNZ appears very uniform at a rotation speed of 400 rpm. Additionally, the hardness in the WNZ increased with increasing rotation speed. No metastable phases are retained in the WNZ, Which means that the aging precipitate strengthening effect has diminished. As the grain size in the WNZ increases with higher rotation speed, the hardness should be decreased according to the hall-patch equation. In previous studies [29, 30], limited dislocation density can lead to much higher contribution to the tensile strength than that of the effect of grain size strengthening contributed to the joint in FSW. Thus, the increase of the dislocation density should be account for the hardness improvement. The lowest hardness is located in the TMAZ on the AS of the joint at the lower rotation speed (e.g., 400 rpm), which is attributed to the inadequate material flow induced in the SRFSW. Meanwhile, the lowest micro-hardness is located in the HAZ on the AS acquired at the higher rotation speed. The lowest hardness is increased with increasing rotation

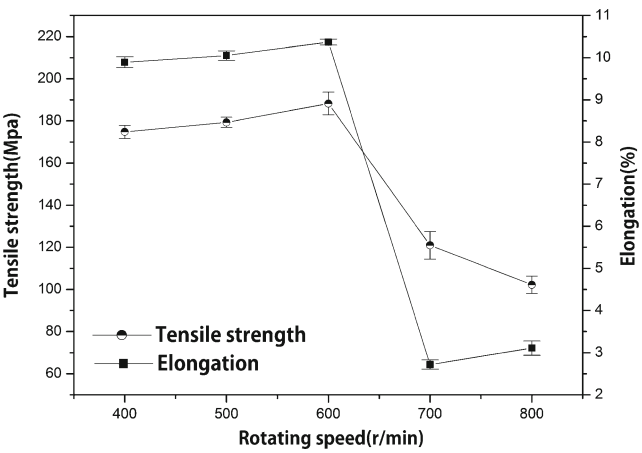

Fig. 6 Tensile properties of the joints welded at different rotation speeds

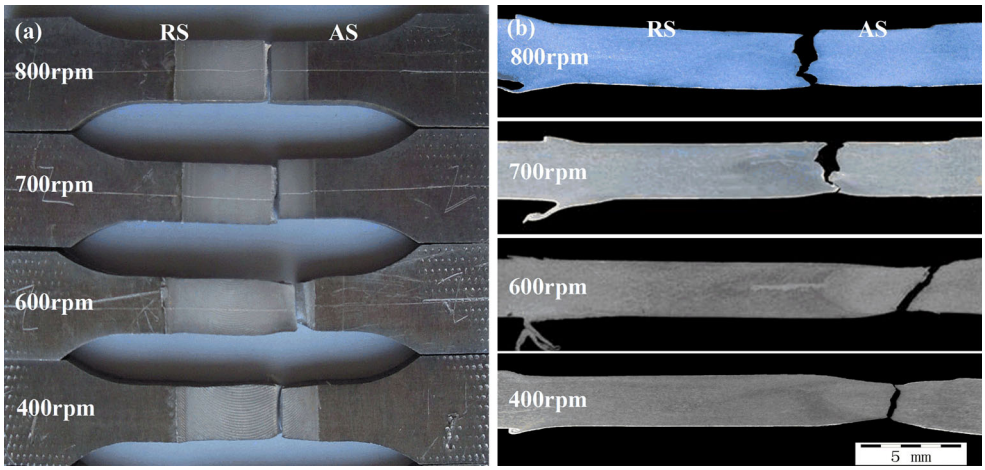

Fig. 7 Fraction features of the joints welded at different rotation speeds: **a** tensile specimens and **b** cross-sections

speed ranging from 400 to 600 rpm. Generally, dissolution and coarsening of the precipitation phases in the HAZ of the precipitation hardened aluminium alloys SRFSW joints are dramatically worsened with the higher heat exposure at the higher rotation speed. Consequently, the lowest hardness is decreased with the increasing rotation speed.

3.3 Tensile properties

The transverse tensile properties of the joints are evaluated with the results displayed in Fig. 6. From the figure, it can be seen that the tensile strength increases with increasing rotation speed when the rotation speeds are lower. Additionally, the maximum value 188 MPa is obtained with the joint efficiency equal to 66 %. The tensile strength evidently decreases as the rotation speed is reached to higher value (e.g., 700 and 800 rpm) as a result of the formation of the void defect.

Clearly, the FSW joint is a heterogeneous composite and is composed of different component parts, including their interfaces. Moreover, the low global elongations obtained for the SRFSW joint is attributed to that the plasticity is confined in the very narrow soften area. As for the 6061 SRFSW joint in the present study, the WNZ/TMAZ interface on the AS becomes smoother as the rotation speed increases. The shaper interface gained at lower rotation speed causes a mismatch material deformation in the WNZ and the TMAZ, decreasing the plastic deformation ability of the joint, and thus the elongation increases with increasing rotation speed in the range of 400–600 rpm as shown in Fig. 6.

The fracture locations vary significantly with the rotation speeds as shown in Fig. 7. For the defect-free joint, the joint are fractured in the TMAZ at the lower rotation speed of 400 rpm consistent with the lowest hardness region of the joint. Moreover, the WNZ/TMAZ interface on the AS tends to be sharper at the lower rotation speed. At the higher rotation speed of 600 rpm, the tensile fracture location shifts from TMAZ to the HAZ on the AS, corresponding to the weakest hardness region in the joint. When the rotation speed further increases up to 700 and 800 rpm, the void defects are formed resulting in that the fracture location moves to the WNZ.

All in all, the rotation speed should be chosen in a reasonable range to produce high quality joints via SRFSW technique. Increasing rotation speed can introduce sufficient material flow in the WNZ, and increase the harden strain in the WNZ and TMAZ. In this case, the tensile fracture shifts from TMAZ to the HAZ on the AS. However, the mechanical properties of the joints decrease to a considerably low level owing to the formation of the void defects when the rotation speed is increased excessively (e.g., 700 and 800 rpm).

4 Conclusions

In this study, the effect of rotation speed on the microstructure and mechanical properties of the joints is investigated by using self-reacting FSW tool with different lower and upper shoulder diameters. From the results and discussion mentioned above, the following conclusions can be drawn.

1. When the upper shoulder diameter is fixed as 18 mm, the weld visual quality is improved with increasing lower shoulder diameter up to 16 mm. At a constant welding speed of 150 mm/min, defect-free joints are produced when the rotation speed is in the range of 400–600 rpm. Much higher rotation speeds (e.g., 700 and 800 rpm) can lead to the formation of the void defects.
2. The grain size and dislocation density in the WNZ of the joint increase with increasing rotation speed. All metastable precipitates are diminished in WNZ of the joint. The hardness increases with increasing rotation speed because the dislocation density plays much more important role than the grain size.
3. The tensile strength increases with the increase of rotation speed in the range of 400–600 rpm, and the maximum joint efficiency is obtained at 600 rpm. When the rotation

speed further increases, the tensile strength decreases sharply as a result of the formation of void defects.

4. The joints welded at lower rotation speeds are fractured in the TMAZ as a result of the sharper WNZ/TMAZ interface and the lowest hardness value. As the rotation speed increases, the fracture location shifts to HAZ corresponding to the lowest hardness location.

Acknowledgments The authors are grateful for the support provided by the National Natural Science Foundation of China (51175117), by the National Basic Research Program of China (2010CB731704) and by the National Science and Technology Major Project of China (2010ZX04007-011).

References

1. Çam G, Koçak M (1998) Progress in joining of advanced materials—Part II: joining of metal matrix composites and joining of other advanced materials. Sci Technol Weld Join 3(4):159–175
2. Pakdil M, Çam G, Koçak M, Erim S (2011) Microstructural and mechanical characterization of laser beam welded AA6056–Al Alloy. Mater Sci Eng A 528(24):7350–7356
3. Çam G, Koçak M (1998) Progress in joining of advanced materials. Int Mater Rev 43(1):1–44
4. Çam G, Ventzke V, dos Santos JF, Koçak M, Jenneguin G, Gonthier-Maurin P, Penasa M, Rivezla C (1999) Characterization of laser and electron beam welded Al-Alloys. Prakt Metallogr 37(2):59–89
5. Çam G, Koçak M (2007) Microstructural and mechanical characterization of electron beam welded Al-Alloy 7020. J Mater Sci 42(17): 7154–7161
6. Çam G, Ventzke V, dos Santos JF, Koçak M, Jennequin G, Gonthier-Maurin P (1999) Characterization of electron beam welded aluminum alloys. Sci Technol Weld Join 4(5):317–323
7. İpekoğlu G, Erim S, Gören Kiral B, Çam G (2013) Investigation into the effect of temper condition on friction stir weldability of AA6061 Al-alloy plates. Kovove Mater 51(3):155–163
8. Liu HJ, Li JQ, Duan WJ (2013) Friction stir welding characteristics of 2219-T6 aluminum alloy assisted by external non-rotational shoulder. Int J Adv Manuf Technol 64:1685–1694
9. İpekoğlu G, Gören Kiral B, Erim S, Çam G (2012) Investigation of the effect of temper condition on friction stir weldablility of AA7075 Al-alloy plates. Mater Technol 46(6):627–632
10. Horton KR (2011) Microhardness, strength and strain field characterization of self-reacting friction stir and plug welds of dissimilar aluminum alloys. PhD thesis, Alabama University, Alabama
11. Taylor DE (2009) Effects of processing parameters on the embrittlement of self-reacting friction stir welds. Bachelor Engineering, Louisiana State University, Louisiana, MS thesis
12. Otsuka D, Sakai Y (2008) Self-reacting pin tool application for railway car body assembly. Proceedings of the 7th International Symposium on Friction Stir Welding, May 20–22, Awaji Island, Japan
13. Marie F, Alléhaux D, Esmiller B (2004) Development of the bobbin tool technique on various aluminum alloys. Proceedings of the 5th International Symposium on Friction Stir Welding, September 14–16, Metz, France
14. Marie F, Guerin F, Deloison D, Aliaga D, Desrayaud C (2008) Investigation on bobbin tool friction stir welding of 2000 series aluminum thin sheets. Proceedings of the 7th International Symposium on Friction Stir Welding, May 20–22, Awaji Island, Japan
15. Mishra RS, Mahoney MW (2007) Mechanical Properties of Friction Stir Welded Aluminum Alloys. In: Mishra RS, Mahoney M W (eds), Friction stir welding and processing. ASM International, pp 7–35
16. Liu HJ, Zhao YQ, Hou JC, Zhang CQ (2010) Method and apparatus for self reacting friction stir welding tool with unequal diameters of the upper shoulder and bottom shoulder, China Patent Application No. ZL 2010 10296480.2
17. İpekoğlu G, Erim S, Çam G (2014) Effects of temper condition and post weld heat treatment on the microstructure and mechanical properties of friction stir butt welded AA 7075 Al-Alloy plate. Int J Adv Manuf Technol 70(1):201–213
18. İpekoğlu G, Erim S, Çam G (2014) Investigation into the influence of post welded heat treatment on the friction stir welded AA 6061 Al-Alloy plates with different temper conditions. Metall Mater Trans A 45A(2):864–877
19. Neumann T, Zettler R, Vilaca P, dos Santos JF, Quintino L (2007) Analysis of self-reacting friction stir welds in a 2024-T351 alloy. In: Mishra RS, Mahoney MW, Lienert TJ, Jata KV (eds) Friction stir welding and processing IV. Wiley, Hoboken, NJ, pp 171–176
20. Toskey A, Arbegas W, Allen C, Patnaik A (2005) Fabrication of aluminum box beams using self-reacting and standard fixed pin friction stir welding. In: Mahoney MW, Mishra RS, Lienert TJ (eds) Jata K V. Friction stir welding and processing III, TMS, pp 171–178
21. Lafly AL, Alléhaux D, Marine F, Donne CD, Döker H (2006) Microstructure and mechanical properties of the aluminum alloy 6056 welded by friction stir welding techniques. Weld World 50:1–13
22. Zhang Z, Liu YL, Chen JT (2009) Effect of shoulder size on the temperature rise and the material deformation in friction stir welding. Int J Adv Manuf Technol 45:889–895
23. Sakthivel T, Sengar GS, Mukhopadhyay J (2009) Effect of welding speed on microstructure and mechanical properties of friction stir welded aluminum. Int J Adv Manuf Technol 43:468–473
24. Ramulu PJ, Narayanan RG, Kailas SV, Reddy J (2013) Internal defect and process parameter analysis during friction stir welding of Al 6061 sheets. Int J Adv Manuf Technol 65:1515–1528
25. Arora KS, Pandey S, Schaper M, Kumar R (2010) Effect of process parameters on friction stir welding of aluminum alloy 2219-T87. Int J Adv Manuf Technol 50:941–952
26. Schneider JA, Nunes AC, Brendel MS (2010) The influence of friction stir weld tool form and welding parameters on weld structure and properties: nugget bulge in self-reacting friction stir welds. Proceedings of the 8th International Symposium on Friction Stir Welding, May 18–20, Timmendorfer Strand, Germany
27. Murr LE, Liu G, McClure JC (1998) A TEM study of precipitation and related microstructures in friction sitir welded 6061 aluminium. J Mater Sci 33(5):1243–1251
28. Sauvage X, Muñoz AC, Dédé A, Huneau B (2008) Precipitate stability and recrystallisation in the weld nuggets of friction stir welded Al–Mg–Si and Al–Mg–Sc alloy. Mater Sci Eng A 491(1–2):364–371
29. Starink MJ, Deschamps A, Wang SC (2008) The strength of friction stir welded and friction stir processed aluminum alloy. Scr Mater 58(5):377–382
30. Woo W, Balogh L, Ungár T, Choo H, Feng ZL (2008) Grain structure and dislocation density measurements in a friction-stir welded aluminum alloy using X-ray peak profile analysis. Mater Sci Eng A 498(1–2):308–313